



TECHNICAL ARTICLE

# A Cu-Ni-Ti Alloy with Excellent Softening Resistance Combined with Considerable Hardness and Electrical Conductivity Obtained by the Traditional Aging Process

YU SUN,<sup>1,2,3</sup> DONGDONG LV,<sup>1,2,3</sup> JINPING LIU,<sup>1,2,3</sup> CHENGJUN GUO,<sup>1,2,3</sup>  
SHENGDA GUO,<sup>1,2,3,4</sup> and JIANBO ZHANG<sup>1,2,3,5</sup>

1.—School of Materials Science and Engineering, Jiangxi University of Science and Technology, Ganzhou 341000, Jiangxi, China. 2.—National Rare Earth Function Materials Innovation Center, Ganzhou 341100, China. 3.—Jiangxi Advanced Copper Industry Research Institute, Yingtan 335000, China. 4.—Jiangxi Yaosheng Tungsten Co, Ltd, Ganzhou 341100, China. 5.—e-mail: zhang4318@163.com

To obtain a copper alloy with a higher softening temperature, a Cu-Ni-Ti alloy was obtained by the traditional smelting method. And, on this basis, we discuss the effects of atom percentages of different Ni-Ti alloys and the mass percent of Ni + Ti on the properties of single-stage aging of Cu-Ni-Ti alloys at 600°C. The results indicate that the alloy with a Ni/Ti atomic ratio of 2 and a total Ni + Ti content of 3 wt.% exhibits the best performance match. After aging at 600°C for 8 h, the Cu-Ni-Ti alloy's softening temperature exceeded 720°C. This property surpasses that of most age-hardened copper alloys. The corresponding hardness and conductivity were 171 HV and 58% IACS, respectively, which is slightly lower than the commonly used time-reinforced copper alloy. After calculation, the Cu-Ni-Ti alloy with a Ni:Ti atomic ratio of 2 and a total Ni + Ti content of 3 wt.% is referred to as the Cu-2.13Ni-0.87Ti alloy. Transmission electron microscopy observations indicated that the precipitated phase in the aged Cu-2.13Ni-0.87Ti alloy consists of dispersed nanoparticles of Ni<sub>3</sub>Ti, which have a semi-coherent interface relationship with the matrix. Upon holding the peak-aged Cu-2.13Ni-0.87Ti alloy at different temperatures for 1 h, it was noted that the precipitates exhibited significant coarsening. Furthermore, when the holding temperature surpassed 700°C, the rate of coarsening increased significantly, accompanied by a rapid decline in hardness.

## INTRODUCTION

Resistance welding electrodes, generator collector rings, and other copper alloy devices must perform in high-temperature environments, demanding exceptional properties such as high-temperature resistance, strength, and hardness. The challenge of maintaining high-temperature softening resistance in copper alloys is particularly demanding.<sup>1,2</sup> Traditional approaches typically involve integrating trace amounts of chromium, zirconium, cobalt,

beryllium, and other alloying elements into copper materials, coupled with aging treatment, to enhance softening temperature resistance.<sup>3</sup>

The precipitation phase, consisting of nanometer-sized particles, developed during the aging treatment, imparts age-hardening copper alloys with exceptional strength and electrical conductivity.<sup>4,5</sup> However, as the high-temperature process progresses, the interface relationship between the precipitation phase and the matrix gradually shifts from coherent or semi-coherent to incoherent, while the size of the precipitation phase simultaneously increases, resulting in a continuous decline in strength. Subsequently, the thermal stability of the age-hardening phase emerges as the significant

factor for the high-temperature softening resistance of age-hardening copper alloys. At present, some typical age-reinforced copper alloys, such as Cu-Ni-Si,<sup>6</sup> Cu-Cr-Zr,<sup>7</sup> Cu-Fe-P,<sup>8</sup> and Cu-Ni-Be,<sup>9</sup> have been applied, whose strengthening phases are Ni<sub>2</sub>Si<sup>10</sup> phase, Cr-rich phase, Fe<sub>2</sub>P<sup>11</sup> phase, and Cu-Be<sup>12</sup> phase, respectively, all of which bring good mechanical and electrical properties to the corresponding alloys. Good mechanical and electrical conductivity, for example, C70250 alloys, C18510 alloys, and C10410 alloys, can reach 255HV/44%IACS, 140HV/80%IACS, and 147HV/68.65%IACS, respectively.

However, due to the influence of recrystallization<sup>13</sup> and precipitation phase coarsening,<sup>14</sup> the softening resistance temperature of commercial age-hardening copper alloys is generally low. For example, Cu-Cr-Zr,<sup>7</sup> Cu-Ni-Si,<sup>15</sup> and Cu-Fe-P<sup>8</sup> softening resistance temperatures of 550°C, 500°C, and 440°C, respectively, for electrodes with Cu-Ni-Be (C17510) alloy softening resistance can reach 600°C. However, the trace beryllium vapor generated during the melting and the heat treatment of beryllium-containing copper materials can have a sizeable toxic effect on the human body and the environment. There is no suitable copper alloy to replace the high-temperature softened beryllium nickel copper alloy.

The aging temperatures of Cu-Ni-Si,<sup>15</sup> Cu-Cr-Zr,<sup>7</sup> and Cu-Fe-P<sup>8</sup> alloys range from 400°C to 550°C. Higher aging temperatures or high-temperature processes above the aging temperature will lead to the rapid transformation of the interface relationship and rapid coarsening of the precipitation phase, resulting in rapid weakening of the aged strengthening effect, which is one of the fundamental reasons for the low anti-high-temperature softening temperature of these alloys. This paper studies the impact of Ni and Ti element ratio and content on the organizational properties of Cu-Ni-Ti alloys in the aging state. It found that the series alloys still have a good age-hardening effect and excellent resistance to high-temperature softening properties when treated at 600°C, and maintain a high level of electrical conductivity. The microscopic characteristics of the main strengthening phases of the peak aging alloys and the effect of high-temperature holding on the coarsening process of the precipitation phase are further analyzed. This study compensates for the shortcomings of common copper alloy high temperature softening capacity, the results of this study providing a new candidate material for copper alloys for high-temperature applications.

## EXPERIMENTAL

The Cu-Ni-Ti alloy was prepared by adding Cu (99.95 wt.%), Ni (99.5 wt.%), and Cu-Ti intermediate alloys in a vacuum induction furnace between 1200°C and 1300°C. The chemical composition of

the molten alloy ingots is shown in Table I. The samples were homogenized at 800°C for 24 h and then hot-rolled, after which the samples were subjected to solid-solution treatment at 950°C for 1 h, followed by immediate quenching in water at room temperature. The quenched samples were isothermally aged at 600°C for 0.5–14 h.

The hardness of the aged samples was tested using a 200HVS-5 Vickers hardness tester with a load of 500 g and a holding time of 15 s. The conductivity of the ancient samples was tested using a Sigma 2008B1C digital eddy current metal conductivity tester. The thermal insulation treatment on the peak-aged samples (1 h at 550–750°C), and their hardness were measured. The size, quantity, and morphology of the second phase in the alloy samples were observed by SEM and TEM; the approximate distribution of the second phase and the content and distribution of Ni and Ti elements in the second phase were analyzed by EDS spectroscopy; HNO<sub>3</sub> and CH<sub>3</sub>OH were used to prepare electrolytic double injection at 3:1 volume ratio and the TEM samples. The microstructure of the samples was observed by TEM (TecnaiG2-20) at 200-KV voltage and the phase diffraction pattern was analyzed.

## RESULTS AND DISCUSSION

Figure 1 shows the effect of different Ni/Ti ratios (1–6) on the performance of Cu-Ni-Ti alloys aged at 600°C with a Ni + Ti content of 3 wt.%. As shown in Fig. 1a, Cu-Ni-Ti alloys with different Ni/Ti ratios exhibit typical time-hardening effects. That is, as the aging time increases, the hardness of the alloy gradually increases to a peak and then slowly decreases. The peak hardness of the alloy with a Ni/Ti atomic ratio of 2 is the highest, reaching 171 HV. As can be seen from Fig. 1b, with the extension of aging time, the conductivity of alloys with different Ni/Ti ratios first increases and then stabilizes. And, as the Ni/Ti ratio increases, the conductivity of the alloy first rises and then falls. The conductivity of the Cu-Ni-Ti alloy with a Ni/Ti atomic ratio of 2 is higher than 58% IACS, which is significantly higher than that of other alloys. As shown in Fig. 1c, after holding for 1 h at different temperatures, the hardness of the aged Cu-Ni-Ti alloys decreases slowly at first and then rapidly with increasing temperature, and the alloys show excellent high-temperature softening resistance properties. The initial hardness of the Cu-Ni-Ti alloy with a Ni/Ti ratio of 2 was 171 HV, and its hardness was 137 HV after holding at 720°C for 1 h. Therefore, after aging treatment at 600°C, the Cu-Ni-Ti alloy with a Ni/Ti atomic ratio of 2 has the best performance, with a peak hardness of 171 HV, a conductivity of 58% IACS, and a softening temperature of 720°C. Its high-temperature softening resistance property is far beyond that of typical

**Table I. Nominal composition of Cu-Ni-Ti alloy**

Number	Ni + Ti = 3 wt.%	Number	Ni/Ti atomic ratio of 2
1	Ni/Ti atomic ratio is 1, copper surplus	7	Ni + Ti = 1 wt.%, copper surplus
2	Ni/Ti atomic ratio is 2, copper surplus	8	Ni + Ti = 2 wt.%, copper surplus
3	Ni/Ti atomic ratio is 3, copper surplus	9	Ni + Ti = 3 wt.%, copper surplus
4	Ni/Ti atomic ratio is 4, copper surplus	10	Ni + Ti = 4 wt.%, copper surplus
5	Ni/Ti atomic ratio is 5, copper surplus	11	Ni + Ti = 5 wt.%, copper surplus
6	Ni/Ti atomic ratio is 6, copper surplus	12	Ni + Ti = 6 wt.%, copper surplus

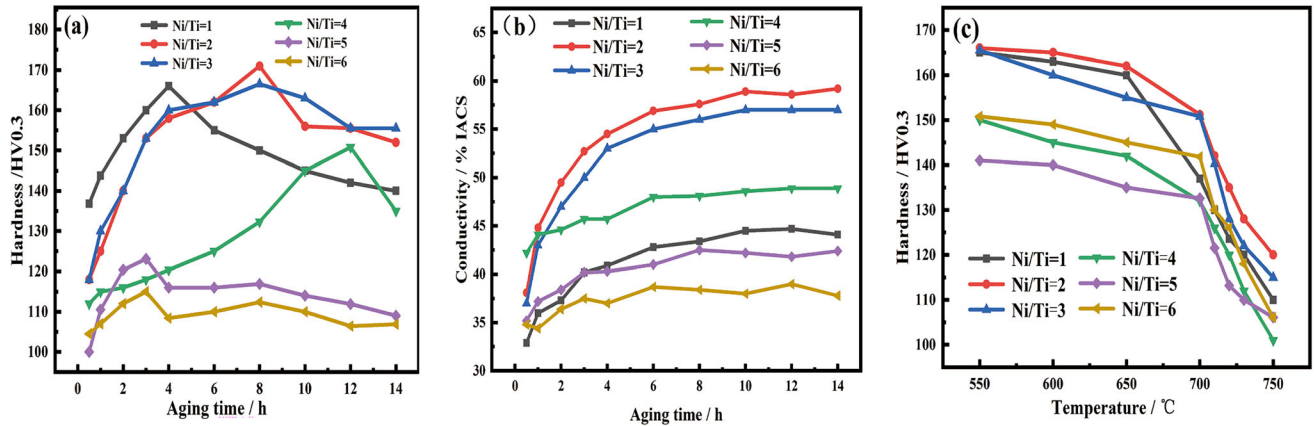


Fig. 1. Effects of different Ni/Ti ratios (Ni + Ti content = 3%) on the performance of Cu-Ni-Ti Alloys in 600°C aging state: (a) time of limitation versus hardness; (b) time of regulation versus conductivity; (c) insulation temperature versus hardness.

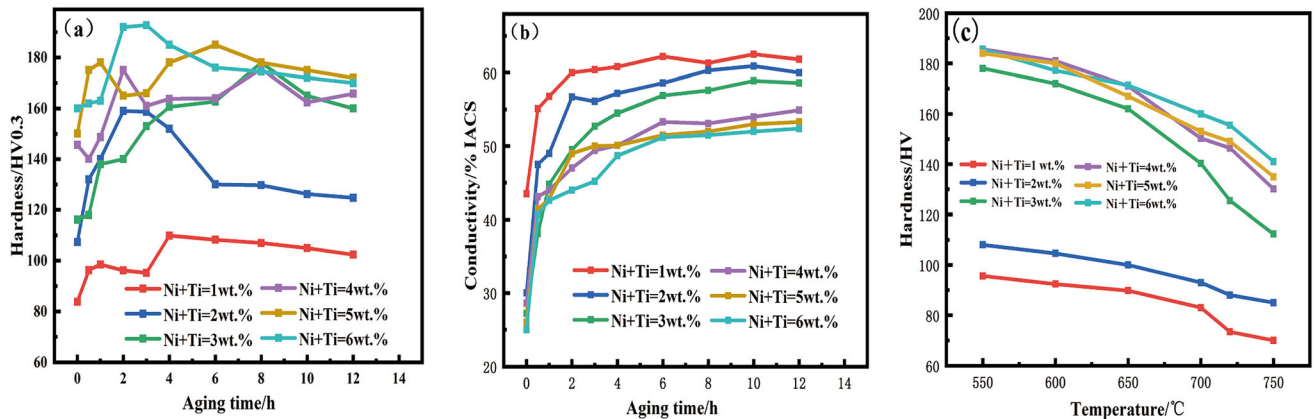


Fig. 2. Effects of different Ni and Ti total content (2 atom ratio of Ni/Ti) on the properties of Cu-Ni-Ti alloys at 600°C time state: (a) time of limitation versus hardness; (b) time of limitation versus conductivity; (c) insulation temperature versus hardness.

age-hardened copper alloys such as Cu-Ni-Si,<sup>15</sup> Cu-Cr-Zr,<sup>7</sup> and Cu-Fe-P,<sup>8</sup> and it maintains high hardness and conductivity.

The hardness versus ageing time, conductivity versus ageing time, and hardness versus temperature of the Cu-Ni-Ti alloys with a Ni:Ti atomic ratio of 2 and a total Ni and Ti contents ranging from 1 wt.% to 6 wt.% are shown in Fig. 2a–c, respectively. As observed, the hardness of the alloys with varying Ni + Ti compositions exhibits a trend of initial increase followed by a decrease. Specifically, alloys with Ni + Ti = 3 wt.% and Ni + Ti = 4 wt.%

reach their peak hardness after 8 h of aging, achieving values of 172 HV and 169 HV, respectively, and the electrical conductivity for these alloys can reach 57% IACS and 52% IACS, respectively. However, the alloy with Ni + Ti = 3 wt.% has a higher resistance to softening, with a temperature of 730°C, compared to 700°C for the alloy with Ni + Ti = 4 wt.%. Therefore, the performance of the Cu-Ni-Ti alloy with Ni + Ti = 3 wt.% is optimal.

Figure 3a shows the performance curves of Cu-Ni-Ti alloys with different Ni/Ti atomic ratios reaching peak aging for a certain total Ni and Ti

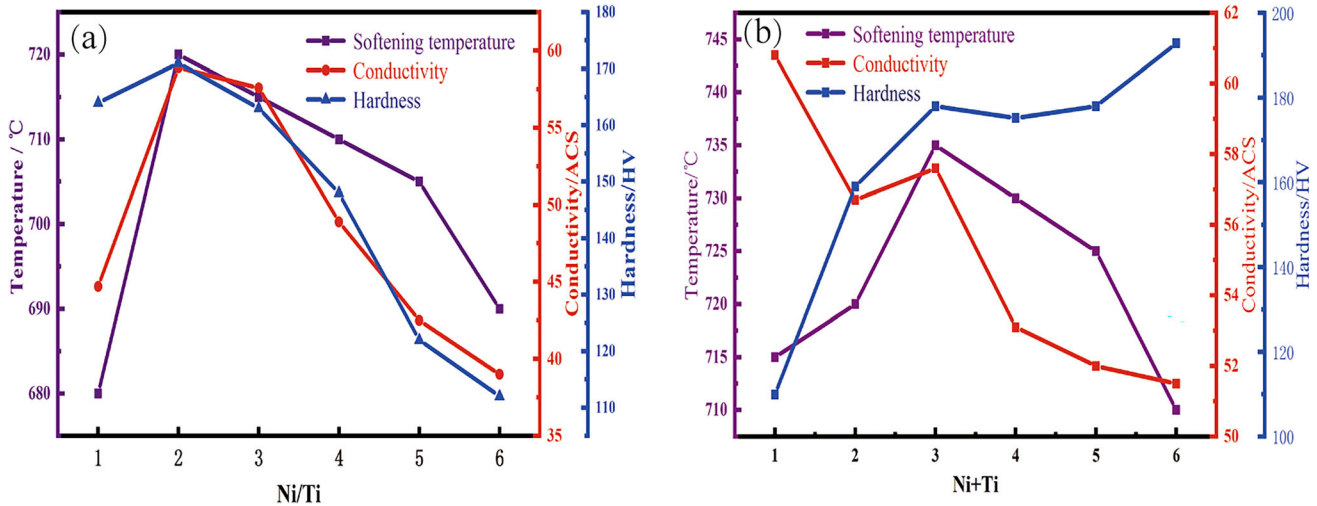


Fig. 3. Cu-Ni-Ti alloy peak aging performance trend: (a) peak aging performance of alloys with different Ni/Ti atomic ratios; (b) peak aging performance of alloys with different total Ni + Ti content.

Table II. Comparison of properties of common copper alloys

	Hardness (HV)	Conductivity (% IACS)	Softening temperature (°C)
Cu-Ni-Si	255	44	500
Cu-Cr-Zr	140	80	550
Cu-Fe-P	147	68.65	400
Cu-Ni-Ti	171	58	720

content. Figure 3b shows the performance curves of Cu-Ni-Ti alloys with different Ni + Ti total contents reaching peak aging for Ni/Ti = 2. It is easy to see that the alloy performance is optimal when the Ni/Ti atomic ratio is 2 and Ni + Ti = 3 wt.%, which is consistent with the results of the performance curves studied above. Table II shows a comparison of the properties of copper-nickel-titanium alloys with those of other common copper alloys.

Figure 4 shows SEM images and EDS for atomic ratio images of Cu-Ni-Ti cast alloys with Ni + Ti = 3 wt.% and 1, 2, 3, and 4 atomic ratios. The images show that the four alloys with different compositions are all constituted by matrix grains and micrometer-sized second-phase particles. Some of these second-phase particles are distributed along the grain boundaries, while a minor portion is dispersed within the grains. Composition analyses of the substrate, the second phase of the crystal boundary, and the second phase particles of the four alloys were carried out, and the results are shown in Table III.

From the figure, the “c” pointing area in Fig. 4 consists primarily of the Cu element. The proportion is higher than 95%, and the content of the Ni and Ti elements is low. To determine the substrate of the alloy, “a” points to the region corresponding to the crystal boundary, and the second phase particles are distributed along the grain boundary, where Ni and Ti are compared to the elemental composition of

the matrix. The introductory content has increased, and the copper content has decreased, but the copper element content at the four alloy boundaries is higher than 95 at.%. The results of the energy spectrum analysis are likely to be influenced by substrates on both sides of the grain boundary; “b” points to a region of second-phase particles located within the crystal. The content of copper in the constituent elements is significantly lower than in the matrix and crystal boundary. The Ni and Ti elemental content significantly increased, and the Ni and Ti atom ratios are close to 3:1, equivalent to the Ni<sub>3</sub>Ti phase of the Ni/Ti atom ratio. Based on the Cu-Ni-Ti phase diagram in the literature, we can determine the primary second phase of the Cu-Ni-Ti alloy to be the Ni<sub>3</sub>Ti phase.<sup>16,17</sup>

In order to clarify the composition of the alloy with excellent overall performance, an alloy with Ni + Ti = 3 wt.% and 2 atomic ratios was selected for analysis, and the alloy composition was calculated to be Cu-2.13Ni-0.87Ti. The results of transmission electron microscopy analysis of the as-cast organization are shown in Fig. 5. As can be seen from Fig. 5a, the organization of the alloy contains a large number of micron-scale second-phase particles. Some of the more significant flaky second-phase distributions are arranged at right angles to each other, as shown by the head of the arrow (a). Other plate-like second-phase particles with a smaller diameter are present independently, as

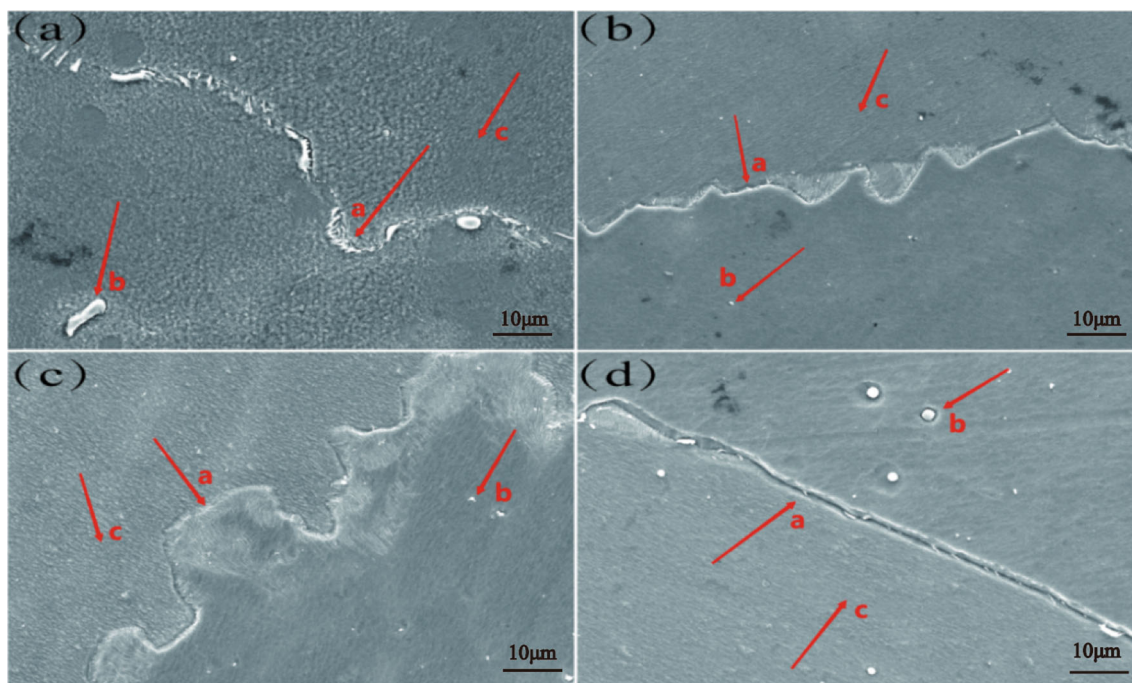


Fig. 4. Cu-Ni-Ti alloy cast SEM organization with different atom ratios of Ni and Ti: (a) Ni/Ti = 1; (b) Ni/Ti = 2; (c) Ni/Ti = 3; (d) Ni/Ti = 4.

**Table III. Cast alloy matrix and second-phase energy spectrum analysis results**

The experiment of alloy	Test point	Atom fraction/at.%		
		Cu	Ni	Ti
Cu-Ni-Ti (Ni:Ti atomic ratio 1)	a	95.32	3.37	1.31
	b	20.1	60.5	20.4
	c	98.3	1.3	0.4
Cu-Ni-Ti (Ni:Ti atomic ratio 2)	a	96.1	2.89	1.01
	b	51.56	36.13	12.31
	c	99.1	0.9	-
Cu-Ni-Ti (Ni:Ti atomic ratio 3)	a	96.2	2.7	1.1
	b	47.4	39.32	13.28
	c	98.33	1.17	0.4
Cu-Ni-Ti (Ni:Ti atomic ratio 4)	a	95.77	3.2	1.03
	b	63.6	27.72	8.68
	c	98.9	0.8	0.3

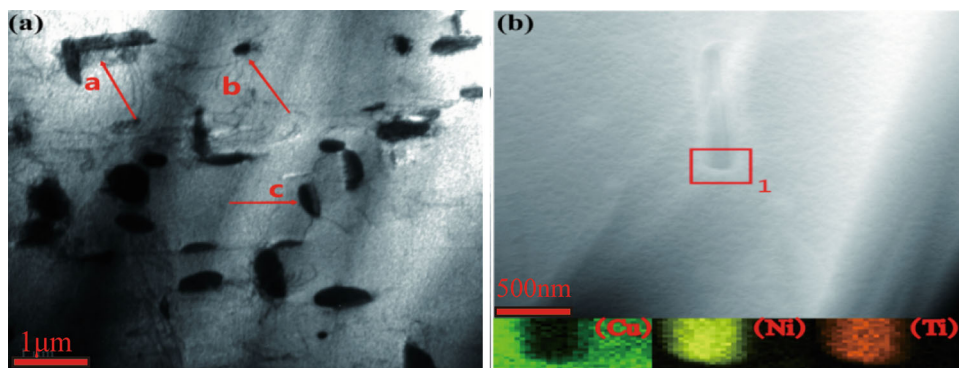


Fig. 5. TEM results for Cu-2.13Ni-0.87Ti cast alloys: TEM image of alloy cast sample; (b) TEM spot sweep results.

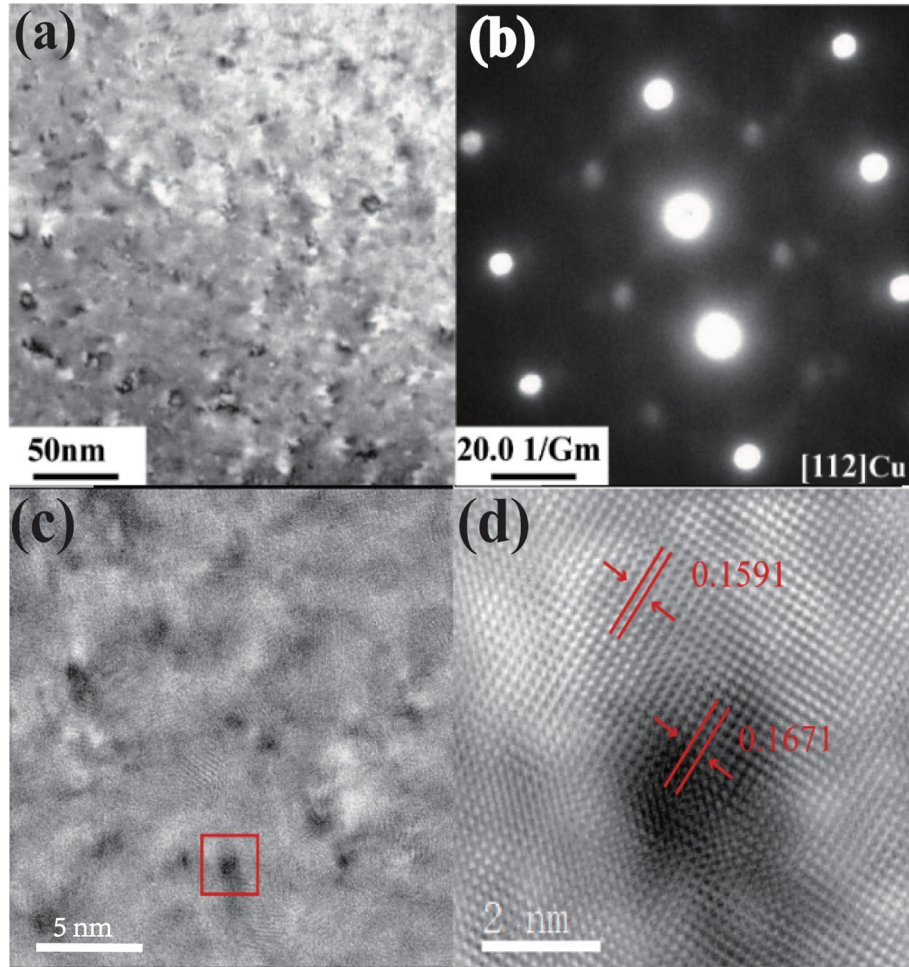


Fig. 6. 600°C/8 h time treatment Cu-2.13Ni-0.87Ti Alloy TEM and HRTEM analyses: (a) peak timeout phase; (b) diffraction patterns of aging samples; (c) high-resolution images of aging states; (d) Fourier-transform of the time state sample.

indicated by arrows (b). As shown in the header, there are a small number of small circular second-phase particles, as shown by the arrow (c). In the typical second-phase particle energy spectrum analysis, surface scan shows that the Ni and Ti elements in the second phase are at a significant concentration peak. At the exact location, the copper element content is significantly reduced.

Figure 6 shows the Cu-2.13Ni-0.87Ti alloy sample TEM and HRTEM results after 600°C/8 h aging. In Fig. 6a, the TEM clear-field phase shows that the nanometer-sized, round-shaped facies of the time-treated sample are dispersed across the copper matrix. In Fig. 6b, the diffraction spots in the direction of  $^{12}$  Cu and the copper matrix are also apparent phase diffraction spots. The lattice constants calibrated as  $a = b = 5.0924 \text{ \AA}$  and  $c = 0.82975 \text{ \AA}$  are essentially the same as the  $\text{Ni}_3\text{Ti}$  phase lattice constant. A high-resolution analysis of the precipitated phase in the high-resolution diagram in Fig. 6c was carried out and the crystal

spacing was 0.1671 nm. The relationship between the matrix and the precipitated phase is characterized by a semi-coherent interface.

Figure 7 shows the sample TEM and HRTEM results after the Cu-2.13Ni-0.87Ti prescription treatment of 720°C insulation of 1 h. Figure 7a shows the clear-field phase of the TEM demonstrating that the spherical precipitation in the sample after the heat insulation treatment of 1 h is significantly coarse compared to that of the aging treatment. In Fig. 7b, with diffraction spots in the direction of  $^{12}$  Cu, in addition to the diffraction spots in the copper matrix, there are still distinct phase diffraction spots, and the lattice constants  $a = b = 5.0911 \text{ \AA}$  and  $c = 0.82988 \text{ \AA}$ . This is consistent with the  $\text{Ni}_3\text{Ti}$  phase lattice constants. High-resolution analysis was performed on the typical precipitated phase in Fig. 7c, and it is shown that the interplanar spacing of the precipitated phase in the aged state is 0.1671 nm, while the interplanar spacing of the matrix is 0.1591 nm. The lattice mismatch between the precipitated phase and the

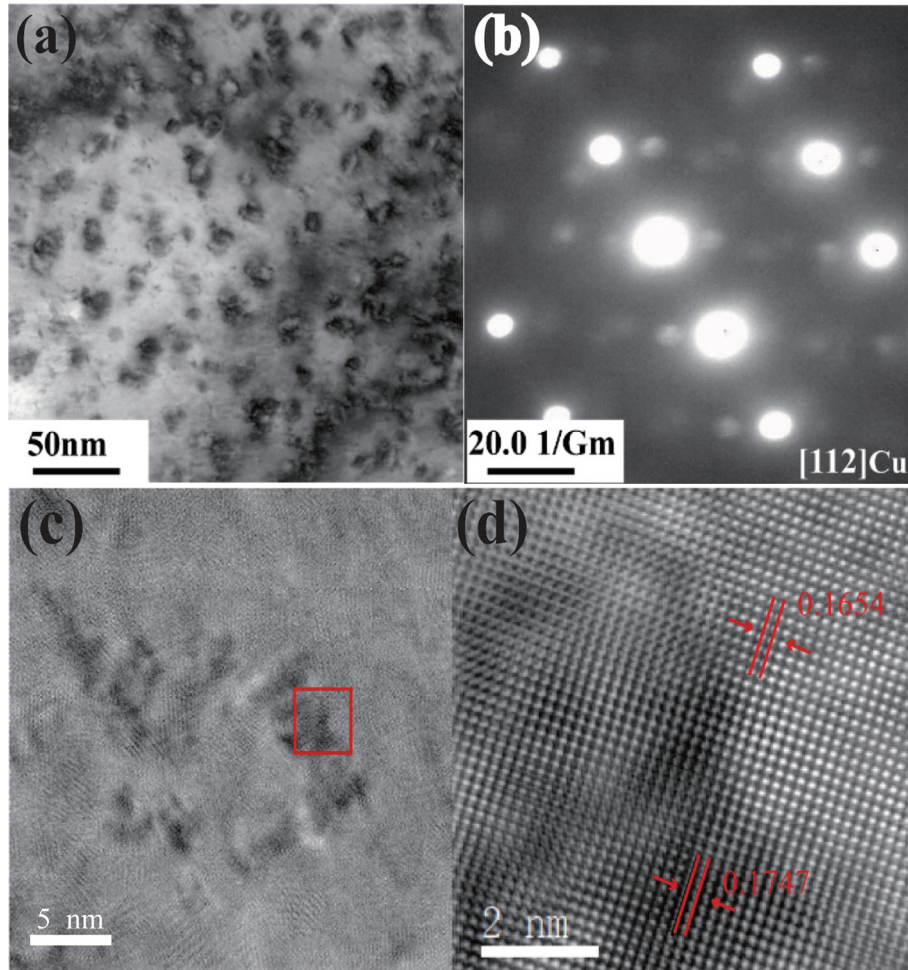


Fig. 7. Cu-2.13Ni-0.87Ti alloy TEM and HRTEM analysis after preserving for 1 h at 720°C: (a) peak timeout phase; (b) diffraction patterns of aging samples; (c) high-resolution image of aging states; (d) Fourier-transform diagram of time state samples.

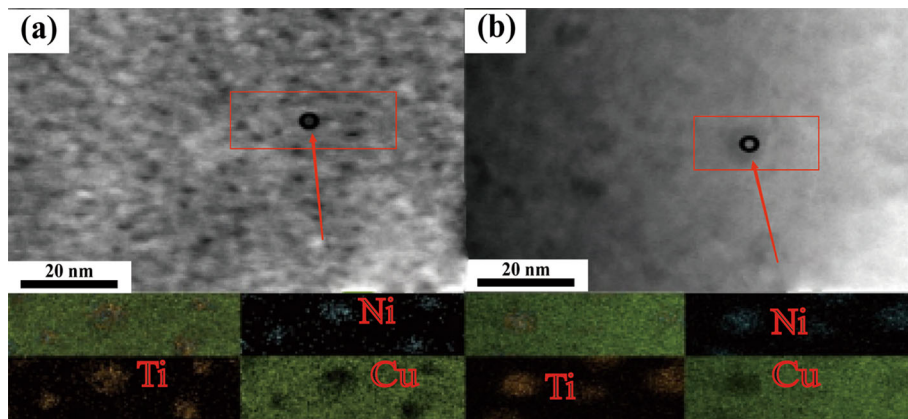


Fig. 8. Analysis of alloy point energy spectrum in different states: (a) 600°C/8 h Cu-2.13Ni-0.87Ti alloy energy spectrum analysis; (b) Cu-2.13Ni-0.87Ti alloy with 720°C insulation of 1 h.

matrix is 5.2%, indicating a semi-coherent interface relationship between the precipitated phase and the matrix.

Figure 8 shows the analysis of the phase energy spectrum components of the Cu-2.13Ni-0.87Ti aging and insulating states, as shown in Table IV. Figure 8a shows that the main components of the nano-precipitate phase in the aging state Cu-Ni-Ti alloy

are Ni and Ti. After point energy spectrum analysis, the Ni element content was 3.4 wt.% and the content of the Ti element was 1.3 wt%. The energy spectrum (Fig. 8b), indicates that the Ni and Ti elements in the Cu-Ni-Ti alloys in the insulation state are still the main components of the disjunctive phase in which significant coarsening occurs. The two elements are visibly pooled at the location of the disjointed stage. The content of Ni and Ti elements in the precipitate phase has been improved compared with the peak-time alloy. The range of Cu elements has decreased, so the diffusion of the Ni and Ti elements from the up slope of the matrix to the disjunctive phase led to the growth of the stage, and the atom ratio of the Ni/Ti element was close to 3:1, equivalent to the peak-time state, also consistent with the phase  $\text{Ni}_3\text{Ti}$  of the atomic ratio.

After aging treatment, the Cu-2.13Ni-0.87Ti alloy exhibited excellent resistance to high-temperature softening. TEM of the 600°C, 650°C, 700°C, and 750°C alloys was performed and the results are shown in Fig. 9, from which it can be observed that the alloy exhibits evenly dispersed distribution due to its high-temperature insulation. Compared with peak-time-effect alloys, the phase size is significantly coarsened. As the temperature increases, the size of the stage increases significantly, from 500°C/1 h 5 nm to 750°C/1 h 20 nm, and the shape

**Table IV. Energy spectrum analysis of precipitate points of alloy peak aging and 1-h holding after peak aging**

	Peak aging state	Heat preservation state
Cu	95.3	94.6
Ni	3.4	3.8
Ti	1.3	1.6

of the phase is gradually changed from spherical to irregular. Notably, 600°C warms to 750°C in equal temperature intervals of 50°C. The precipitate phase coarsening rate due to the insulation process below 650°C is significantly lower than the precipitate coarsening due to the increase from 650°C to 750°C, compared with Fig. 1c The insulation temperature–hardness relationship curve of the alloy shown at the temperature above 700°C after the hardness drop rate is significantly consistent.

## CONCLUSION

Component optimization and traditional aging treatment were used to prepare Cu-Ni-Ti alloys with high softening temperatures and good hardness and conductivity. The influence of primary alloy elemental content and proportions on the aged state performance of the alloy was studied and the morphological and dimensional changes of the main intensified phase species in the heat insulation process were analyzed. The main conclusions are as follows:

1. Different Cu-Ni-Ti alloys with varying Ni and Ti contents exhibit typical age-hardening characteristics during artificial aging at 600°C. The peak-aged Cu-Ni-Ti alloys with Ni/Ti atomic ratio is 2 and Ni + Ti = 3 wt.% have good comprehensive properties, with a Vickers hardness of 171 HV, an electrical conductivity of 58% IACS, and an anti-softening temperature of 720°C
2. After being treated at 600°C/1 h, the main strengthening phase of the Cu-2.13Ni-0.87Ti alloy is a dispersed spherical nanoparticle precipitation phase. Through analysis, it was found that the lattice structure and composition of this strengthening phase are close to  $\text{Ni}_3\text{Ti}$ . The existence of this phase is the key factor for significant improvement in properties such as

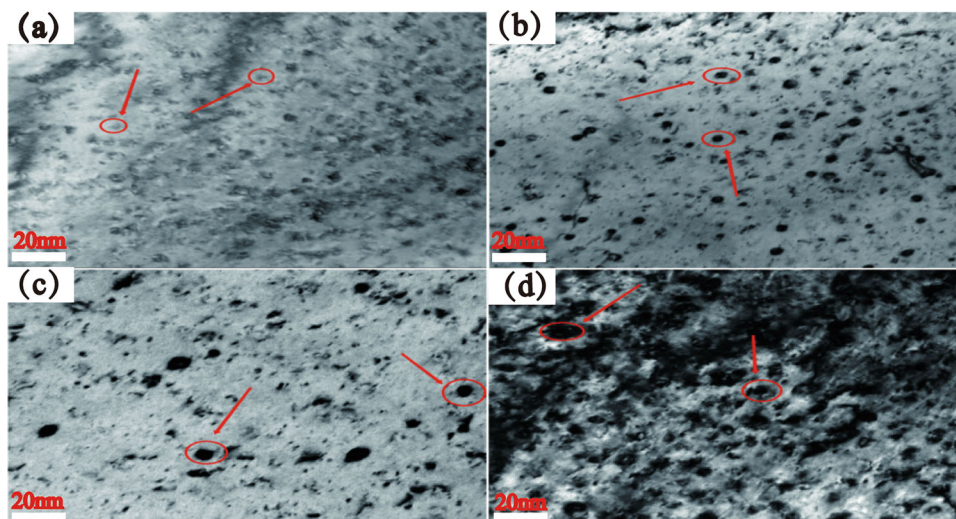


Fig. 9. Cu-2.13Ni-0.87Ti alloy TEM at high-temperature insulation of 1 h: (a) 600°C; (b) 650°C; (c) 700°C; (d) 750°C.



the hardness, conductivity, and softening temperature of the Cu-2.13Ni-0.87Ti alloy.

3. In the peak state Cu-2.13Ni-0.87Ti alloy in the high-temperature insulation process, when the insulation temperature is above 700°C, the hardness of the alloy starts to decrease significantly, and the coarsening rate of the precipitated phase increases significantly. Its Ni/Ti element ratio is still close to Ni<sub>3</sub>Ti.

### ACKNOWLEDGEMENTS

This work was supported by National Copper Smelting and Processing Engineering Technology Research Center (No. 20231ZDD0205) and the Natural Science Foundation of Jiangxi Province (No. 20225BCJ22013).

### AUTHOR CONTRIBUTIONS

Yu Sun: Conceptualization, Methodology, Writing - original draft. Dongdong Lv and Jinping Liu: Data curation, investigation, conceptualization. Chengjun Guo and Shengda Guo: Investigation, Formal analysis. Jianbo Zhang: Supervision, Writing—review and editing.

### CONFLICT OF INTEREST

The authors declare that they have no known competing financial interests or personal relationships that could have appeared to influence the work reported in this paper.

### REFERENCES

1. A.M. Sadoun, M.M. Mohammed, A. Fathy, and O.A. El-Kady, *J. Market. Res.* 9(3), 5024 (2020).
2. C. Li, W. Zeng, Y. Xie, J. Wang, J. Liang, R.E. Logé, and D. Zhang, *Mater. Sci. Eng. A* 778 (2020).

3. A.G. Raab, D.A. Aksenov, R.N. Asfandiyarov, I.S. Kodirov, and G.I. Raab, *IOP Conf. Ser. Mater. Sci. Eng.* 447, 012088 (2018).
4. S. Asgari, R. Sharghi-Moshtaghin, M. Sadegh Ahmadi, and P. Pirouz, *Philos. Mag.* 93(10–12), 1351 (2013).
5. H.S. Ren, X. Wu, B. Chen, H.P. Xiong, and Y.Y. Cheng, *Weld. World* 61(2), 375 (2017).
6. Y. Cao, S.Z. Han, E.-A. Choi, J.H. Ahn, X. Mi, S. Lee, H. Shin, S. Kim, and J. Lee, *J. Alloys Compd.* 843, 156006 (2020).
7. J.S. Chen, B. Yang, J.F. Wang, X.P. Xiao, H.M. Chen, and H. Wang, *Mater. Res. Express* 5(2), 51 (2018).
8. Q.Y. Dong, L.N. Shen, F. Cao, Y.L. Jia, K.J. Liao, and M.P. Wang, *J. Mater. Eng. Perform.* 24(4), 1531 (2015).
9. Y.J. Zhou, K.X. Song, J.D. Xing, and Y.M. Zhang, *J. Alloys Compd.* 658, 920 (2016).
10. W.N. Liao, X.F. Liu, Y.H. Yang, and M. Du, *Mater. Sci. Eng. A* 767(1), 38428 (2019).
11. Q.M. Dong, *Heat Treat. Met.* 30, 182 (2005).
12. L.J. Peng, B.Q. Xiong, G.L. Xie, Q.S. Wang, and S.B. Hong, *Rare Met.* 32(4), 332 (2013).
13. I.Z. Awan, and A.Q. Khan, *J. Chem. Soc. Pak.* 41(1), 1 (2019).
14. J.H. Su, S.G. Jia, F.Z. Ren, P. Liu, and B.H. Tian, *Adv. Mater. Res.* 79–8(2), 1507 (2009).
15. Y.L. Jia, Y. Pang, J. Yi, Q. Lei, Z. Li, and Z. Xiao, *J. Alloys Compd.* 942, 169033 (2023).
16. W.J. Zhu, L.I. Duarte, and C. Leinenbach, *Calphad* 47, 9 (2014).
17. H. Zhang, Y. He, F. Yang, H. Liu, and Z. Jin, *Thermochim. Acta* 574, 121 (2013).

**Publisher's Note** Springer Nature remains neutral with regard to jurisdictional claims in published maps and institutional affiliations.

Springer Nature or its licensor (e.g. a society or other partner) holds exclusive rights to this article under a publishing agreement with the author(s) or other rightsholder(s); author self-archiving of the accepted manuscript version of this article is solely governed by the terms of such publishing agreement and applicable law.